INTERNATIONAL JOURNAL FOR NUMERICAL METHODS IN FLUIDS
Int. J. Numer. Meth. Fluids 2003; **43**:301–318 (DOI: 10.1002/fld.611)

3D free-surface flow computation using a RANSE/Fourier–Kochin coupling

Pierre-Emmanuel Guillerm[1,*,†] and Bertrand Alessandrini[2,‡]

[1]*Department of Ocean Engineering, Florida Atlantic University, 777 Glades Road, Boca Raton, FL 33431, U.S.A.*
[2]*Ecole Centrale de Nantes, Laboratoire de Mecanique des Fluides, Division Hydrodynamique Navale, 1 rue de la noe, 44321 Nantes Cedex 3, France*

SUMMARY

A coupling method for numerical calculations of steady free-surface flows around a body is presented. The fluid domain in the neighbourhood of the hull is divided into two overlapping zones. Viscous effects are taken in account near the hull using Reynolds-averaged Navier–Stokes equations (RANSE), whereas potential flow provides the flow away from the hull.

In the internal domain, RANSE are solved by a fully coupled velocity, pressure and free-surface elevation method. In the external domain, potential-flow theory with linearized free-surface condition is used to provide boundary conditions to the RANSE solver. The Fourier–Kochin method based on the Fourier–Kochin formulation, which defines the velocity field in a potential-flow region in terms of the velocity distribution at a boundary surface, is used for that purpose. Moreover, the free-surface Green function satisfying this linearized free-surface condition is used.

Calculations have been successfully performed for steady ship-waves past a serie 60 and then have demonstrated abilities of the present coupling algorithm. Copyright © 2003 John Wiley & Sons, Ltd.

KEY WORDS: free-surface flows; Reynolds-averaged Navier–Stokes equations; Fourier–Kochin method; steady ship-waves problem

1. INTRODUCTION

Main features of the flow around ship hull are existence of a three-dimensional turbulent boundary layer, presence of a free-surface wave pattern and its interaction with the boundary layer and the wake. The viscous and wave effects can be calculated using Reynolds-averaged Navier–Stokes equations (RANSE) with appropriate free-surface boundary conditions. However, this computation requires a large number of grid nodes and amount of CPU time to achieve solution in the entire flow field [1]. Moreover, this solution is perturbed by the decreasing concentration of nodes away from the hull. Since viscous effects are confined to a

*Correspondence to: P.-E. Guillerm, Department of Ocean Engineering, Florida Atlantic University, 777 Glades Road, Boca Raton, FL 33431, U.S.A.
†E-mail: guillerm@oe.fau.edu
‡E-mail: bertrand.alessandrini@ec-nantes.fr

Received 5 August 2002
Revised 27 May 2003

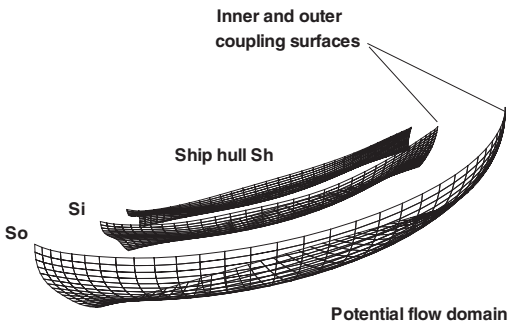

Figure 1. Sketch of the coupling surfaces.

small region surrounding the hull and the wake, a zonal approach which combines viscous flow near the hull and potential theory away from the ship can therefore be an effective method to solve ship free-surface problems.

In the present paper, steady flows around a body are studied. RANSE are solved by a fully coupled velocity, pressure and free-surface elevation method [2] in the internal domain. In the external domain, the Fourier–Kochin method [3, 4], proposed by Noblesse, which defines the velocity field in a potential-flow region in terms of the velocity distribution at a boundary surface, is used. The great advantage of this method is that the three components of the velocity on the boundary surface are used to provide fluid characteristics in the potential domain. So this method seems to be well suited to make the coupling successful. Fluid domain is divided into two overlapping zones (Figure 1). In the inner domain, bounded by the ship hull S_h and the surface S^o, RANSE and continuity equation are written through a partial transformation from Cartesian space (x^i) to curvilinear space (ξ^i) fitted to the hull and the free-surface at each time. General discretization method is based on second-order (in space and time) implicit finite differences. The fully coupled system is solved by iterative algorithm using matrix preconditioning. The fluid domain is then re-gridded using the new free-surface wave pattern. In the potential-flow domain, located outside S^i, the Fourier–Kochin formulation of Green function satisfying this linearized free-surface condition is used to provide boundary condition for the RANSE calculation. Velocity components on S^i are computed from the viscous flow solution (Figure 1), and used as velocity distribution at the boundary surface of the potential domain. Potential calculation provides wave field pattern in the outer region and velocities and pressure on the viscous boundary surface S^o.

The coupling approach was already used for steady ship-waves problem. Tahara and Stern [5] have coupled RANSE method with a source/doublet Dawson method. A displacement–body concept was used to take into account viscous effects in the potential calculation, but this method cannot be used in the presence of flow separation. Campana *et al.* [6] have discretized the RANSE by a finite volume method in the neighbourhood of the hull and they have used the linearized model of Dawson in the potential domain. The external flow is splitting in a double model flow and a perturbation term. So they first compute an iterative RANSE/potential double-body solution, then the free-surface flow is computed. This solution is consistent with the potential formulation, but requires iterating RANSE and potential calculations twice; first the double-body calculation and then with the free-surface effects

accounted for. Moreover, only the normal component of the velocity on the matching surface is computed from the viscous flow solution and then used as Neumann condition for the potential-flow problem. Chen *et al.* [7] use the same solution, but they iterate with the complete (with free surface) RANSE and potential solutions from the beginning, using the complete RANSE velocity on the matching surface as boundary condition for the double-body and free surface potential calculations. This procedure requires only one iterating calculation, but velocities used as boundary conditions for the double-body calculation are no longer 'double-body' velocities. Chen *et al.* couple a fully non-linear Laplace solver and an RANSE solver to compute 2D diffraction problems [8] and steady ship flows [9]. Normal component of the velocity on the matching surface, computed from the viscous flow solution, are used as Neumann condition for the Laplace solver. This solution is consistent with the viscous computation but a 3D mesh is required in the outer domain.

In this paper, authors have applied the viscous–potential coupling to steady ship-waves problem. Aims of using such hybrid method is the CPU time and memory safe, and to avoid numerical damping away from the ship. The purpose of this paper is then to show abilities of this new viscous–potential coupling approach.

2. RANSE SOLVER

2.1. Governing equations

The convective form of RANS equations is written through a partial transformation from Cartesian space (x^1, x^2, x^3) to curvilinear space (ξ^1, ξ^2, ξ^3) fitted to the hull and the free surface at each iteration. Free-surface elevation, the three Cartesian velocity components (u^i), pressure (p) including gravitational effects $(\rho g x^3)$ and turbulent kinetic energy $(2/3\rho k)$ are the dependant unknowns [2].

Mean momentum transport equations are written in a moving referential attached to the hull:

$$u^\alpha_{,t} + (a^j_i(u^i - u^i_g) - \nu_{\text{eff}} f^j - a^i_k \nu_{t,i} a^j_k) u^\alpha_{,j} + \frac{1}{\rho} a^k_\alpha p_{,k} - \nu_{\text{eff}} g^{ij} u^\alpha_{,ij} - a^i_k \nu_{t,i} a^\alpha_j u^k_{,j} + q_i = 0 \tag{1}$$

where (a^i) is the contravariant basis, (g^{ij}) the contravariant metric tensor, (f^i) the control grid functions and (u^i_g) the grid velocity which traduces the displacement of the mesh. Inertia forces due to non-Galilean referential (rotating motion, accelerated translation) are taking into account in the (q_i) terms. In translation case (with or without drift angle) inertia forces are expressed as follows where U is the hull velocity:

$$\begin{aligned} q^1 &= q^1_d = U_{,t} \cos(\theta) \\ q^2 &= q^2_d = U_{,t} \sin(\theta) \\ q^3 &= q^3_d = 0 \end{aligned} \tag{2}$$

Mass conservation is expressed as the classical continuity equation:

$$a^j_i u^i_{,j} = 0 \tag{3}$$

To close the set of equations, we use a classical k–ω model proposed by Wilcox [10–12], introducing a specific dissipation rate ϖ without low Reynolds formulation requirement. Transport equations of turbulent kinetic energy and dissipation rate are written as follows:

$$(a_i^j(u^i - u_g^i) - (\nu + \sigma^* \nu_t) f^i - a_k^i \sigma^* \nu_{t,i} a_k^j) k_{,j} - (\nu + \sigma^* \nu_t) g^{ij} k_{,ij} - Pr + \beta^* \varpi k + k_{,t} = 0 \tag{4}$$

$$(a_i^j(u^i - u_g^i) - (\nu + \sigma \nu_t) f^i - a_k^i \sigma \nu_{t,i} a_k^j) \varpi_{,j} - (\nu + \sigma \nu_t) g^{ij} \varpi_{,ij} - \gamma \varpi \, Pr/k + \beta \varpi^2 + \varpi_{,t} = 0 \tag{5}$$

with

$$\nu_t = \gamma^* \frac{k}{\varpi} \tag{6}$$

and

$$\begin{aligned} \beta &= 3/40; \quad \sigma = 0.5; \quad \gamma = 5/9 \\ \beta^* &= 0.09; \quad \sigma^* = 0.5; \quad \gamma^* = 1 \end{aligned} \tag{7}$$

2.2. Boundary conditions

On walls, no-slip boundary conditions are applied. The hull is assumed to be fixed in the referential attached to the hull. Then, boundary conditions on the hull are

$$u^i = 0 \tag{8}$$

Symmetry conditions are used in the $(x^1 O x^3)$ plane. As the hull geometry is symmetric in this plane, we assume that the flow is also symmetric in this plane. On the symmetry plane, boundary conditions are

$$u^1_{,2} = 0, \quad u^3_{,2} = 0, \quad u^2 = 0 \tag{9}$$

Lastly, outer limits of the computational domain are assumed to be far enough, therefore the flow is not perturbed by the hull. The fluid is then assumed at rest on outer boundary. In the referential attached to the hull, we get:

$$u^1 = U, \quad u^2 = 0, \quad u^3 = 0 \tag{10}$$

When the coupling procedure is used, the outer limit of the Navier–Stokes computational domain corresponds to the outer coupling surface S^o and then, velocity components will be computed from the potential-flow solver using the Fourier–Kochin approach.

2.3. Free-surface conditions

Free-surface boundary conditions are one kinematic condition, two tangential dynamic conditions and one normal dynamic condition. The kinematic condition, coming from the continuity

hypothesis, expresses that the fluid particles of the free surface stay on it:

$$h_{,t} + (b_i^j(u^i - u_g^i)h_{,j})_{(i,j)\in\{1,2\}} - u^3 = 0 \tag{11}$$

where b^i is the bidimensional contravariant basis.

Dynamic conditions are given by the continuity of strains at the free surface. If the pressure is assumed to be constant above the free surface, the normal dynamic condition is

$$p - \rho g h - 2\frac{\rho \nu_{\text{eff}}}{|a^3|^2} a_i^3 a_j^3 a_j^k u_{,k}^i - \frac{\gamma}{r} = 0 \tag{12}$$

where γ is the superficial tension coefficient (that is a physical way to smooth the free surface near the hull) and r the free-surface medium curvature radius. Tangential dynamic conditions are simply given by a linear combination of first-order velocity derivatives:

$$a_{\alpha i} g^{j3} u_{,j}^i = 0 \tag{13}$$

2.4. Discretization

General discretization is based on second-order (in space and time) implicit finite differences. Discrete unknowns are distributed on a structured curvilinear grid fitted to the hull and the free surface. Velocity Cartesian components, kinetic turbulent energy and specific dissipation rate are located on grid nodes. Pressure is located at the centre of each elementary volume and free-surface elevation is located at the centre of free-surface interfaces.

Convection terms are computed using an upwind second-order scheme on a 13-nodes molecule. Diffusion terms need seven nodes for second-order derivatives and 12 nodes to express cross second-order derivatives (Equation (1)) while pressure gradient requires eight nodes for each component [2, 13].

The pressure equation is computed from the continuity equation by evaluating the divergence of momentum equations. The Rhie and Chow interpolation technic [14] is used to avoid even–odd uncoupling [2].

Concerning free-surface calculation, it has been shown that the classical way using normal dynamic condition as Dirichlet condition on pressure and uncoupled kinematic equation as transport equation to compute free-surface elevation induces some issues arising from difficulties to exactly solve mass conservation under the free-surface [2]. Efficient solution consists in using a fully coupled algorithm [2] that requires at each iteration the linear solution of mean momentum equations, continuity equation and whole boundary conditions including free-surface condition.

$$\begin{pmatrix} M_{11} & M_{12} & M_{13} & M_{14} \\ M_{21} & M_{22} & 0 & 0 \\ 0 & M_{32} & M_{33} & 0 \\ 0 & 0 & M_{43} & M_{44} \end{pmatrix} \begin{pmatrix} U \\ \tilde{U} \\ P \\ H \end{pmatrix} = \begin{pmatrix} fu \\ f\tilde{u} \\ fp \\ fh \end{pmatrix} \tag{14}$$

Unfortunately, most efficient iterative algorithms (CGSTAB+ILU, Multigrid) are unable to invert this system due to the very bad matrix conditioning of the pressure block M_{33}. The solution consists in modifying the system using free-surface boundary conditions to express

the flux through the free surface. In this case, conditioning number decreases and fully coupled system becomes invertible by iterative algorithms. Resulting linear system for velocity (U) and pseudovelocity ($\tilde{U}$) components, pressure (P) and free-surface elevation (H) is written as follows:

$$\begin{pmatrix} M_{11} & M_{12} & M_{13} & 0 \\ M_{21} & M_{22} & 0 & 0 \\ 0 & M_{32} & M_{33} & 0 \\ 0 & 0 & M_{43} & M_{44} \end{pmatrix} \begin{pmatrix} U \\ \tilde{U} \\ P \\ H \end{pmatrix} = \begin{pmatrix} fu \\ f\tilde{u} \\ fp \\ fh \end{pmatrix} \tag{15}$$

3. POTENTIAL SOLVER

Waves are analysed within the classical linear potential-flow theory. The flow is observed from a moving system of co-ordinates (x, y, z) in steady translation with the mean forward speed U of the ship. The z-axis is vertical and points upward, moreover the undisturbed free surface is taken as the plane $z = 0$. Non-dimensional co-ordinates $\mathbf{x} = (x, y, z)$, time t, velocity potential Φ and related flow variables are defined with respect to the body length L, the acceleration of gravity g and the density of water ρ as basic reference units. The Froude number is defined as $F = U/\sqrt{gL}$.

3.1. General formulation

The velocity potential $\Phi = \Re e\{\phi(\mathbf{x})\}$ satisfies the continuity equation

$$\nabla^2 \Phi = 0 \tag{16}$$

the linear free-surface boundary condition

$$\frac{\partial^2 \Phi}{\partial t^2} + \frac{\partial \Phi}{\partial z} = 0, \quad z = 0 \tag{17}$$

and the radiation condition at infinity

$$\Phi \to 0 \quad \sqrt{x^2 + y^2} \to \infty \tag{18}$$

For steadyship-waves motion the free-surface boundary condition is expressed as

$$F^2 \frac{\partial^2 \Phi}{\partial x^2} + \frac{\partial \Phi}{\partial z} = 0, \quad z = 0 \tag{19}$$

The boundary condition on the inner coupling surface will be provided by the RANSE solver. Namely, components of the viscous velocity-field on the inner coupling surface will be used as velocity distribution by the Fourier–Kochin approach as it will be shown in the following sections.

3.2. Green function

The Green function G, associated with the boundary condition (19), is expressed as the sum of a Rankine term and a free-surface component

$$G = G^S + G^F \tag{20}$$

G^S is defined as

$$4\pi G^S = -\frac{1}{R} + \frac{1}{R'} \tag{21}$$

with

$$R = \sqrt{(x-\xi)^2 + (y-\eta) + ^2 (z-\zeta)^2}$$
$$R' = \sqrt{(x-\xi)^2 + (y-\eta) + ^2 (z+\zeta)^2}$$

G^F is given by the Fourier superposition of elementary waves

$$4\pi^2 G^F = \lim_{\varepsilon \to 0^+} \int_{-\infty}^{+\infty} \int_{-\infty}^{+\infty} \frac{e^{Zk - i(X\alpha + Y\beta)}\, d\alpha\, d\beta}{F^2\alpha^2 - k - i\varepsilon\, \mathrm{sign}(\alpha)} \tag{22}$$

with

$$k = \sqrt{\alpha^2 + \beta^2}$$
$$(X, Y, Z \leqslant 0) = (\xi - x, \eta - y, \zeta + z)$$

$(x, y, z \leqslant 0)$ and $(\xi, \eta, \zeta \leqslant 0)$, respectively, stand for the singularity and flow-observation points.

Furthermore, D is the dispersion function

$$D = (F\alpha)^2 - k \tag{23}$$

3.3. Fourier–Kochin formulation

The Fourier–Kochin formulation and the near-field far-field decomposition of the potential presented in the next sections were initially proposed by Noblesse and Chen [15, 16], we then follow their works here. Thus, practical calculations involve distributions of singularities of the form

$$\wp = \int_{P_0} \begin{Bmatrix} G\sigma \\ \nabla G \cdot \boldsymbol{\delta} \end{Bmatrix} \tag{24}$$

where P_0 stands for a hull panel or a waterline segment near a point $\mathbf{x}_0 = (x_0, y_0, z_0)$ (in present calculations $\mathbf{x}_0$ stands for the middle of hull panel) and σ and $\boldsymbol{\delta} = (\delta_x, \delta_y, \delta_z)$ are source and dipole densities, respectively. In usual approach, G and ∇G are evaluated using (22) and integrated over a panel or a segment as in (24). However, the space integration (with respect to the point $\mathbf{x}$) can be performed first and the Fourier integration (with respect to the Fourier unknowns α and β) last. Thus, the Green function is not evaluated directly in this approach,

which is based on a Fourier representation of the free-surface component of the velocity potential. This approach corresponds to the method used by Kochin [17, 18] for steady-flow problems. For steady ship waves the free-surface component $\wp_{\mathrm{F}}$ is given by the double Fourier integral:

$$4\pi^2 \wp^F = \lim_{\varepsilon \to 0^+} \int_{-\infty}^{+\infty} \int_{-\infty}^{+\infty} \frac{S \mathrm{e}^{Zk - i(X\alpha + Y\beta)} \, \mathrm{d}k \, \mathrm{d}\theta}{F^2 \alpha^2 - k - i\varepsilon \, \mathrm{sign}(\alpha)} \tag{25}$$

$$\frac{4\pi^2}{f^2} \wp^F = \lim_{\varepsilon \to 0^+} \int_{-\pi}^{+\pi} \int_{0}^{\infty} \frac{S \mathrm{e}^{Zk - i(X\alpha + Y\beta)} \, \mathrm{d}k \, \mathrm{d}\theta}{f^2 - k + i\varepsilon} \tag{26}$$

where $(X, Y, Z \leqslant 0) = (\xi - x_0, \eta - y_0, \zeta + z_0)$ and S is the spectrum function defined as

$$S = \int_{P_0} \kappa \left\{ \begin{array}{c} \sigma \\ i\alpha\delta_x + i\beta\delta_y + k\delta_z \end{array} \right\} \tag{27}$$

with $\kappa = \mathrm{e}^{k(z - z_0) + i[\alpha(x - x_0) + \beta(y - y_0)]}$.

For coupling problems, sources and dipoles densities are evaluated on the boundary surface S^{i} and on its intersection curve Γ^{i} with the mean free-surface plane $z = 0$ (Figure 2), using the Green identity. Moreover, these densities can be expressed as functions of the velocity components on S^{i} and Γ^{i} (Figure 2). Namely, the function $S(\alpha, \beta)$ given by Noblesse and Yang [4] is expressed as

$$\begin{aligned} S(\alpha, \beta) = & \int_{S^{\mathrm{i}}} A^{S^{\mathrm{i}}} \, \mathrm{e}^{k(z - zo) + i(\alpha(x - xo) + \beta(y - yo))} \, \mathrm{d}A \\ & - \int_{\Gamma^{\mathrm{i}}} A^{\Gamma^{\mathrm{i}}} \, \mathrm{e}^{-kzo + i(\alpha(x - xo) + \beta(y - yo))} \, \mathrm{d}L \end{aligned} \tag{28}$$

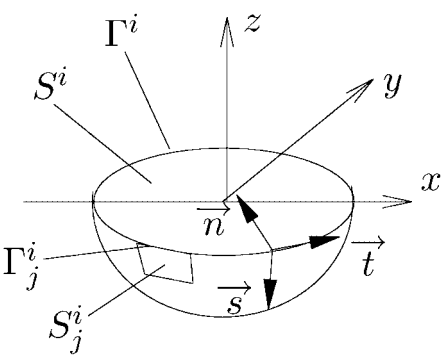

Figure 2. Sketch of the inner coupling surface.

where dA and dL stand for the differential elements of area and arc length of the surface S^i and the curve Γ^i. Functions A^{S^i} and A^{Γ^i} are defined as [4]

$$A^{S^i} = \mathbf{u}\cdot\mathbf{n} + i\left(\frac{\beta}{k}t_x - \frac{\alpha}{k}t_y\right)\mathbf{u}\cdot\mathbf{s} - i\left(\frac{\beta}{k}s_x - \frac{\alpha}{k}s_y\right)\mathbf{u}\cdot\mathbf{t} \tag{29}$$

For steadyship-waves problems, A^{Γ^i} is given by

$$A^{\Gamma^i} = F^2\left(t_y^2\mathbf{u}\cdot\mathbf{n} + \left(t_x t_y + \frac{\alpha\beta}{k^2}\right)\mathbf{u}\cdot\mathbf{t}\right) \tag{30}$$

Velocity vector $\mathbf{u}$ in relations (29) and (30) is given by the boundary condition on the inner coupling surface S^i.

3.4. *Near-field and far-field components*

It is shown by Chen and Noblesse in References [3, 15, 16] that the double Fourier integral (25) (26) can be expressed as the sum of a wave component $\wp^W$, which is dominant in the far field, and a local component $\wp^N$, negligible in the far field but significant in the near field. Thus,

$$\wp^F = \wp^W + \wp^N \tag{31}$$

For steady free-surface flows, the dispersion function D defines two dispersion curves, which are symmetric with respect to both $\alpha = 0$ and $\beta = 0$. The dispersion curves $D = 0$ are given by $\alpha = \pm\alpha_d(\beta)$ where the function $\alpha_d(\beta)$ is defined by $F^2\alpha_d = \sqrt{F^2 k_d}$ with $F^2 k_d = K$,

$$K = 1/2 + \sqrt{1/4 + b^2} \tag{32}$$

and $-\infty < b = F^2\beta < +\infty$. The wave component $\wp^W$ and the local component $\wp^N$ (31) of the free-surface potential (25) can be represented in terms of the speed-scale co-ordinates $(X^u, Y^u, Z^u) = (X, Y, Z)/F^2$.

The wave component given in Reference [16] is

$$\wp^W = \frac{[\mathrm{erf}(X^U) - 1]}{4\pi F^2}\int_{-\infty}^{+\infty} db\,\frac{\sqrt{K}\,\mathrm{e}^{KZ^U}}{\sqrt{0.25 + b^2}} \Im m\left\{S\left(\frac{\sqrt{K}}{F^2}, \frac{b}{F^2}\right)\mathrm{e}^{-i(X^U\sqrt{K} + Y^U b)}\right\} \tag{33}$$

The local component $\wp^N$ can be expressed as [16]

$$2\pi^2 F^2 \wp^N = I^N + \frac{\pi S_0}{\sqrt{(X^u)^2 + (Y^u)^2 + (v - Z^u)^2}} \tag{34}$$

where $S_0 = S(0,0)$ is the value of the spectrum function S at the origin of the Fourier plane, v is a real positive number, and I^N is given by the double Fourier integral [16]:

$$I^N = \Re e \int_{-\infty}^{+\infty} \mathrm{d}b \mathrm{e}^{-iY^u b} \int_0^{\infty} \mathrm{d}a \mathrm{e}^{-iX^u a} \Lambda \tag{35}$$

with Λ defined by Noblesse [16] as

$$\Lambda = \frac{S \mathrm{e}^{cZ^u}}{a^2 - c} - \frac{S_0 \mathrm{e}^{-c(v-Z^u)}}{c} - \frac{\sqrt{K} \mathrm{e}^{KZ^u}}{\sqrt{1+4b^2}} \left(\frac{E^- S^+}{a - \sqrt{K}} - \frac{E^+ S^-}{a + \sqrt{K}} \right) \tag{36}$$

Here $(a,b,c) = F^2(\alpha, \beta, k)$, K is function (32), $E^{\pm}$ are localizing functions defined as

$$E^{\pm} = \mathrm{e}^{-(a \pm \sqrt{K})^2/4} \tag{37}$$

S, S_0 and $S^{\pm}$ stand for

$$S = S(a/F^2, b/F^2) \tag{38}$$

$$S_0 = S(0,0) \tag{39}$$

$$S^{\pm} = S(\pm\sqrt{K}/F^2, b/F^2) \tag{40}$$

4. MATCHING CONDITIONS

The coupling algorithm can only be used with steady flows. During the first part of computations RANSE are computed on the entire flow field. The coupling algorithm is then used when the steady state is established.

Conditions on S^{o} are given by the potential-flow calculation; velocity components on S^{i}, given by RANSE method, are used as velocity distributions for the Fourier–Kochin method to compute velocity and pressure in the inner domain on S^{o} and to compute wave field in the outer domain. Once these calculations are made, a new time step of the RANSE calculation is performed with the updated boundary condition on S^{o}.

In practical computations, surface S^{i} and its intersection curve Γ^{i} with the mean free surface are divided in panels and segments (Figure 2). Velocity is assumed constant on each panel and segment, then the spectrum function can be expressed as a sum on panels and segments:

$$S(\alpha,\beta) = \sum_{j=1}^{\mathrm{np}} \int_{S_j^{\mathrm{i}}} A^{S_j^{\mathrm{i}}} \mathrm{e}^{k(z-zo_j)+\omega_j} \, \mathrm{d}A^j - \sum_{j=1}^{\mathrm{ns}} \int_{\gamma_j^{\mathrm{i}}} A^{\gamma_j^{\mathrm{i}}} \mathrm{e}^{-kzo_j+\omega_j} \, \mathrm{d}L^j \tag{41}$$

where np and ns represent, respectively, number of panels on S^{i} and number of segments on Γ^{i} and $\omega_j = i(\alpha(x - xo_j) + \beta(y - yo_j))$.

Moreover, functions $A^{S_j^{\mathrm{i}}}$ and $A^{\gamma_j^i}$ are written as functions of velocity components on each panel and segment, so by inverting sums on np and ns in (41) with Fourier integrals in (33) and (34), far-field and near-field components can be expressed as sums of functions of the velocity on surface S^{i} and on water-line Γ^{i}, multiplying influence coefficients [19]. These influence coefficients only depend on panels geometry and on flow-observation points. Thus, they are evaluated at the beginning of the computation. When the outer boundary condition on S^{o} is updated, only functions of the velocity are re-evaluated.

The coupling algorithm is used to provide new velocity components on the outer boundary S^{o} of the RANSE solver and to provide pressure in cells closed to the outer surface S^{o}. If only velocity are computed by the coupling method, mass conservation is not verify on cells closed to S^{o} and then computations fail after few time steps. Pressure in these cells is then provided and the mass conservation law is not solved.

5. RESULTS

In order to test the method some numerical applications have been performed. These applications correspond to the steadyship-waves problem studied in previous sections. For this application, a self-consistency test is first performed in order to valid the Fourier–Kochin approach for coupling problems. For self-consistency computations, the potential and its derivatives on a half-sphere surrounding a source are computed. In a second step, these derivatives are used as velocity distributions for the coupling method to compute the potential outside the half-hemisphere. The potential computed by the coupling approach is then compared with the potential directly provided by the source (Figure 3).

Once the coupling method is validated by the self-consistency test, the method is used with the RANSE solver in the inner domain. The flow around the ship hull is separated in two overlapping zones. Near the hull (in the inner domain), RANSE are solved. Away from the hull (in the outer domain), flow is assumed to be potential and the coupling approach is used. The inner domain is located between the hull S_{h} and the outer coupling surface S^{o}, while the outer domain is located outside the inner coupling surface S^{i} (Figure 4). Velocities computed by the RANSE solver on S^{i} are used as velocity distributions for the Fourier–Kochin method

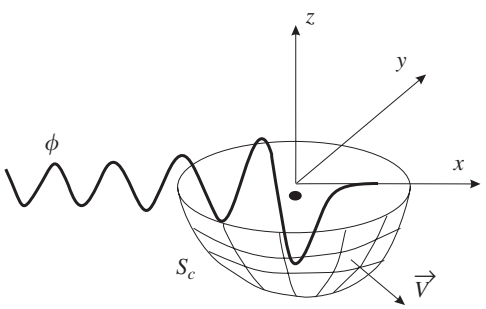

Figure 3. Sketch of the self-consistency test.

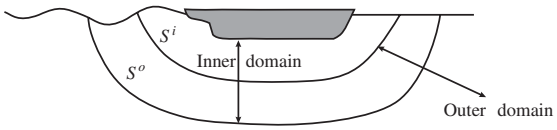

Figure 4. Sketch of coupling surfaces.

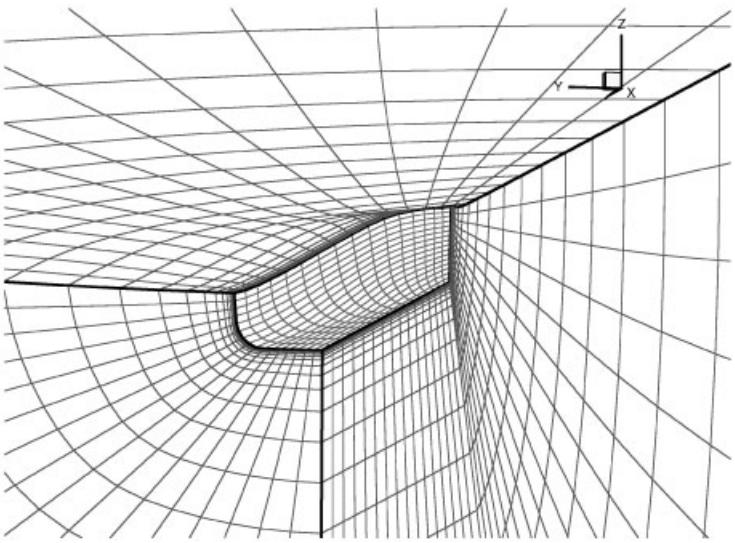

Figure 5. Partial view of the grid around serie 60.

in the outer domain. Specifically, velocities components and pressures on the outer surface S^o are evaluated with the coupling algorithm. A new RANSE computation is then performed with these updated boundary conditions.

Flows around a serie 60 $CB = 0.6$ merchant ship at Froude number $Fn = 0.316$ is studied. Results of the self-consistency test are first presented, then the viscous–potential coupling is studied. Only symmetric cases are studied, hence one-half of the fluid domain around the hull is discretized.

For self-consistency computations, influence of the number of panels on the half-hemisphere and influence of the near-field component of the Green function are studied.

For the coupling calculations O–O grid is used (Figure 5). The grid has 57 nodes in the streamwise direction, 57 nodes in the normal direction and 25 nodes in the girthwise direction. Non-dimensional values are defined with respect to the ship length L, the acceleration of gravity g, the density of water ρ and the hull velocity U_∞.

5.1. Self-consistency test

In a first step, the problem of steady flow past a source is solved with the Fourier–Kochin formulation of the Green function. Green function and velocity are computed on the free surface and on a surface surrounding the source. In a second step, velocity components on

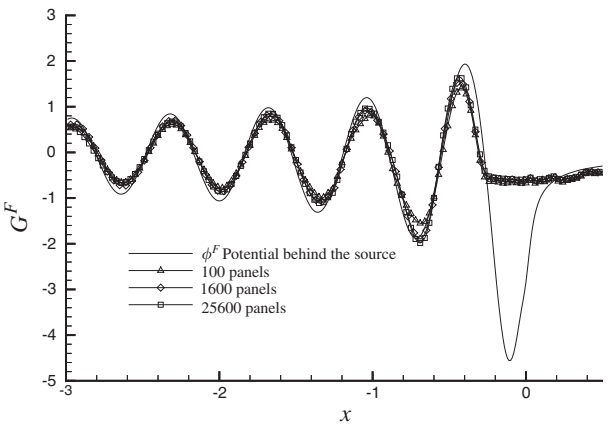

Figure 6. Self-consistency test—Fn = 0.32—influence of the panels number.

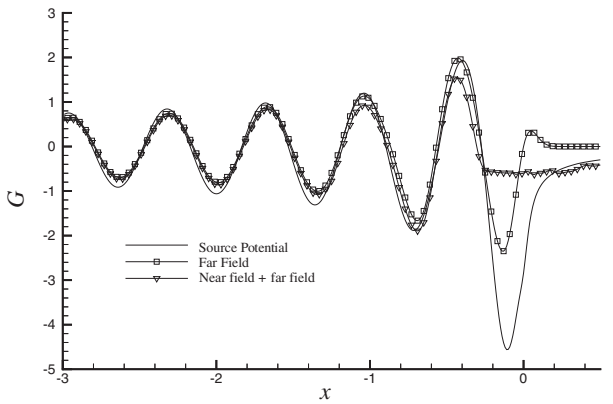

Figure 7. Self-consistency test—Fn = 0.32—influence of the near-field component.

the surface surrounding the source are used to distribute sources and doublets panels over this surface. This second step is then similar to a coupling. Computed velocity potentials behind the source for the two steps are then compared. The half-hemisphere is centred at the origin and its radius is 0.3. The source is located in $(x = 0, y = 0, z = -0.05)$. In Reference [20] Yang *et al.* present results of self-consistency tests on the whole free-surface for two different shape of coupling surface; a half-hemisphere and a half-ellipsoid. Here, results in the wake of the source on the free surface are discussed. Influence of the number of panels on the surface surrounding the source is first presented. This surface is discretized with 100, 1600 and 25 600 panels. Figure 6 show the potential $G^F = G^N + G^W$ behind the source on the free surface.

Figure 6 shows that results of the three computations are in accordance with the source potential and that results for 1600 and 25 600 panels are quite similar. A fine mesh refinement is then not required on the coupling surface.

In Figure 7, influence of the near-field component of the Green function on the coupling is studied. On this picture, results of the self-consistency test are shown by using $G^W + G^N$ and

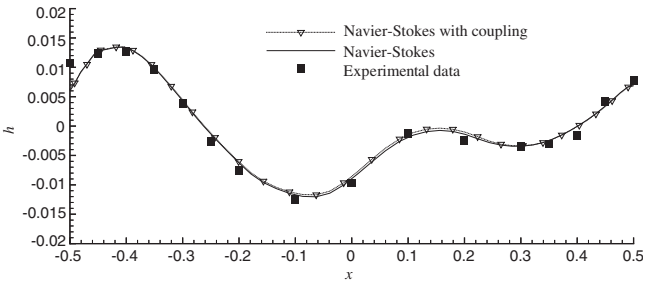

Figure 8. Free-surface elevation on the hull.

only G^W. In this figure, we notice that the near-field component of the Green function is not significant behind the coupling surface except before the source. Moreover, much more time is needed to compute the near-field component of the Green function (about 3 or 4 times), so for viscous–potential coupling this term will not be computed.

5.2. *Viscous–potential coupling*

In this section, numerical results of the coupling procedure are compared with RANSE calculations and with experimental results of Stern *et al.* [21]. All the computations are performed with a Froude number $\mathrm{Fn} = 0.316$ and a Reynolds number $Re = 2.5 \times 10^6$. In the outer domain the Green function has been evaluated for steady ship-boundary conditions, so the coupling algorithm can only be used when the hull has reached its final velocity. For this study the ship is starting from rest and reaches its nominal velocity after 75 time steps. The coupling is performed after 180 time steps and then every time step.

First, results are compared with experimental data to check the accuracy of the coupling method. Then influence of coupling surfaces locations is studied, and results are compared with fully RANSE computations. Lastly, CPU time safe is studied.

5.2.1. Comparison with experimental data. In this section, results of the coupling approach are compared with experimental data of Stern *et al.* [21]. Coupling surfaces S^{i} and S^{o} correspond to 20th and 35th surfaces in the normal direction. Lastly, the inner coupling surface is discretized with 800 panels.

In Figures 8–10, results of the coupling method are compared with fully RANSE computations and with experimental data [21]. Specifically, free-surface elevations on the hull and in two slides $y = C^{st}$ are shown.

In Figures 9 and 10, the dotted line shows the limit between inner and outer domains.

Near the hull (in the inner domain) results of both computations are very closed. So the coupling algorithm does not disturb the inner flow computation. Moreover, we can notice free-surface numerical damping with fully RANSE computations, while with the coupling algorithm there is no damping and numerical results are closed to experimental data (Figure 10).

5.2.2. Location of the inner coupling surface S^{i}. In order to show influence of the inner coupling surface location, two computations are performed with two different inner coupling surfaces. Thus, the outer coupling surface is the 35th surface in the normal direction and the

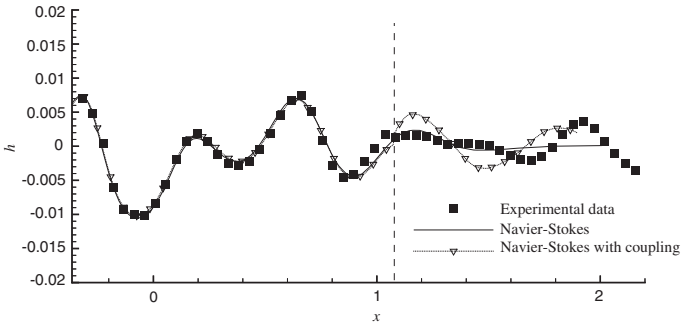

Figure 9. Free-surface elevation on slide $y = 0.1$.

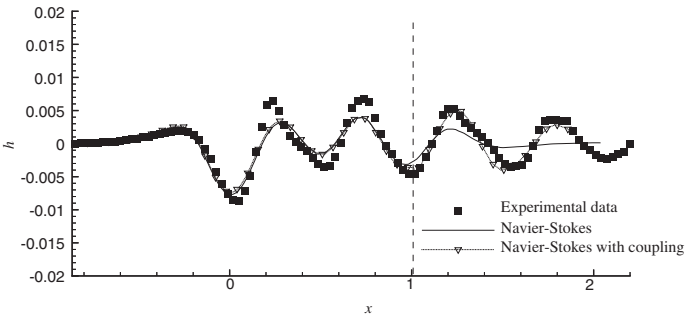

Figure 10. Free-surface elevation on slide $y = 0.2$.

inner coupling surfaces are the 20th and 30th surfaces in the normal direction. Moreover, the inner coupling surface is discretized with 300 panels on the half-surface.

In Plate 1, pressure on the free surface is presented. Black curves represent sights of coupling surfaces on the free surface. Velocity levels are chosen between $+0.9$ and $+1.1$, while pressure levels are chosen between $+100$ and -100. In Plate 1, pressure magnitudes are smaller when the inner coupling surface is far from the hull. Wavelength λ in the wake is evaluated using expression [22]:

$$\frac{\lambda}{L} = 2\pi \mathrm{Fn}^2$$

This gives a wavelength $\lambda/L = 0.6$. For the inner coupling surface $j = 20$, RANSE are solved with 34 cells by wavelength, while for the inner coupling surface $j = 30$, RANSE are solved with 17 cells by wavelength. In the last computation the number of cells on the inner coupling surface seems to small to correctly propagate the wave field far from the hull, then numerical damping occurs in the viscous flow.

This first test shows that the inner coupling surface has to be located close to the hull, where the numerical damping does not influence the RANSE solver. Following [22] at least 30 cells by wavelength are required on the inner coupling surface to ensure wave propagation without damping.

5.2.3. Location of the outer coupling surface S^o. Once the inner coupling surface S^i is chosen, the outer coupling surface S^o has to be located. As for the inner coupling surface, two computations with two different outer coupling surfaces are performed. The inner coupling surface is the 20th surface in the normal direction, while the two outer surfaces correspond to the 25th and 35th surfaces in the normal direction. In Plate 2, non-dimensional pressure on the free surface is presented for the two computations.

Pressure field computed with coupling surfaces $j = 20$ and 25 is on the upper part of the picture and pressure field computed with coupling surfaces $j = 20$ and 35 is on the lower part.

In Plate 2, we notice that non-physical oscillations appear in front of the boat. These oscillations come from the bad resolution of the linear system in the inner domain. Moreover, pressure magnitude in the wake increases when the two surfaces are closed. With the coupling surfaces $j = 20$ and 35, distance between the two surfaces is greater than $\lambda/2$ while with the coupling surfaces $j = 20$ and 25, distance between the two surface is equal to $\lambda/5$. Coupling computations are performed without the near-field component of the Green function, but similar results are obtained if the near-field component is used [19]. The outer coupling surface $j = 25$ seems to be too closed from the hull. Indeed, with the coupling approach, based on potential-flow theory, there is no wake behind the ship (Plate 4). So the coupling algorithm modifies the flow in the wake in the inner domain. If the outer coupling surface is far from the hull, the wake is numerically damped and the outer domain computation has a smaller influence on the flow in the wake in the viscous domain.

The outer coupling surface should be located at more than $\lambda/2$ from the inner coupling surface in order to get a negligible near-field component but also to not cross the wake close to the hull. A good way to overcome this problem would be to performed computations on C–O grid. Then j surfaces would not cross the wake and coupling algorithm would be used on surfaces where both viscosity and curl are negligible.

5.2.4. Comparison with fully RANSE computations. In this section, results of the coupling approach are compared with results of the RANSE solver without coupling. Coupling surfaces S^i and S^o are chosen following conclusions of previous sections and then correspond to 20th and 35th surfaces in the normal direction. Lastly, the inner coupling surface is dicretized with 800 panels. In Plates 3 and 4, velocity in x and pressure on the free surface are presented for the viscous solver and for the coupling approach.

In Plates 3 and 4, numerical damping in the viscous flow is noticed while the coupling approach computes the far-field waves. The coupling algorithm which is based on the potential-flow theory, does not compute the wake in the inner domain. Viscous velocity fields in the wake are slightly perturbed by the coupling algorithm, nevertheless this has no influence on the flow closed to the hull (Figure 8). As mentioned previously, computations on C–O grids will overcome this problem. Moreover, Figures 11(a) and 11(b) show computations stability.

Figure 11(a) shows that CPU time decreases of a factor 3 when the coupling algorithm is used. When the coupling is used, the Navier–Stokes grid is reduced so the number of unknowns in the linear system is reduced as well. Moreover, 11(b) shows that solver iterations by time step decrease when the coupling algorithm is used. As for the CPU time, the linear system to solve is smaller, then the solver reaches convergence faster.

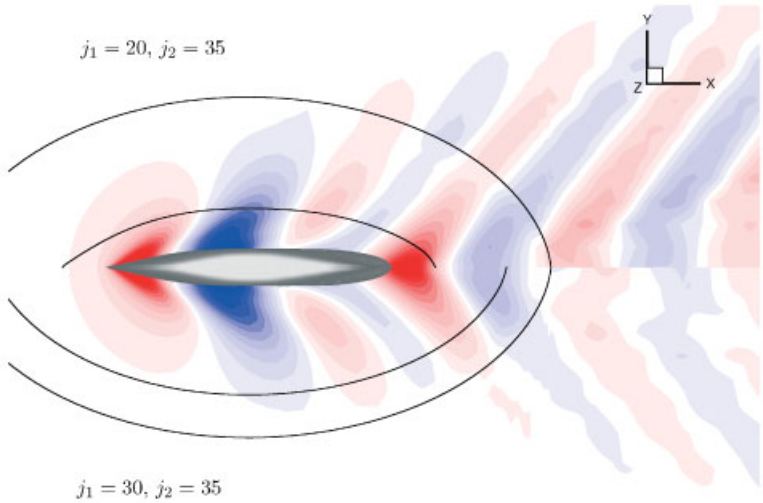

Plate 1. Pressure on the free surface with $\mathrm{Fn} = 0.316$—influence of the location of S^i.

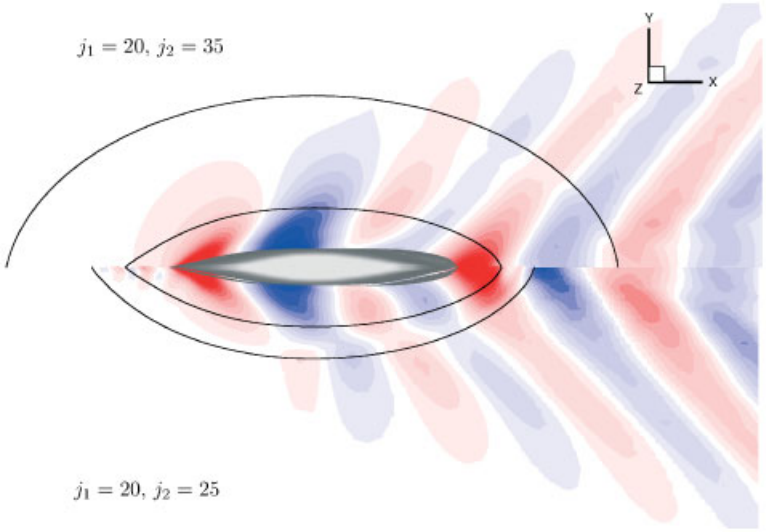

Plate 2. Pressure on the free surface for $\mathrm{Fn} = 0.316$—influence of the outer surface location.

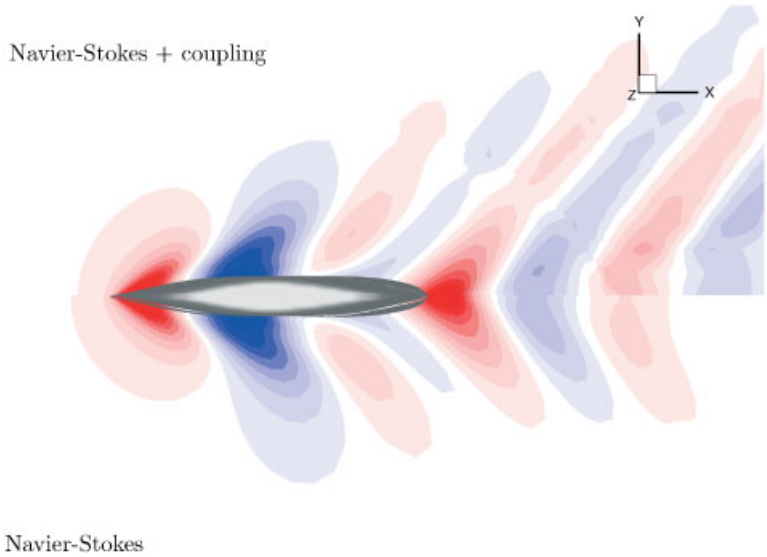

Plate 3. Pressure on the free surface with Fn = 0.316—comparison with fully RANSE computation.

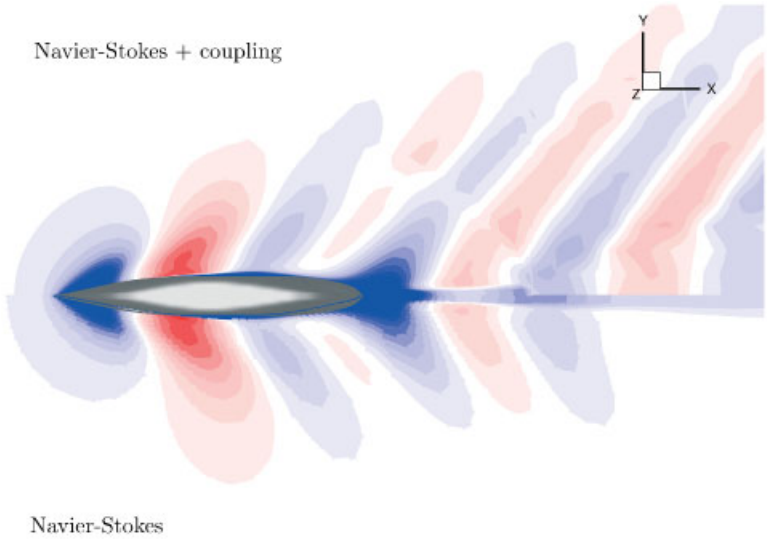

Plate 4. Velocity in x on the free surface with Fn = 0.316—comparison with fully RANSE computation.

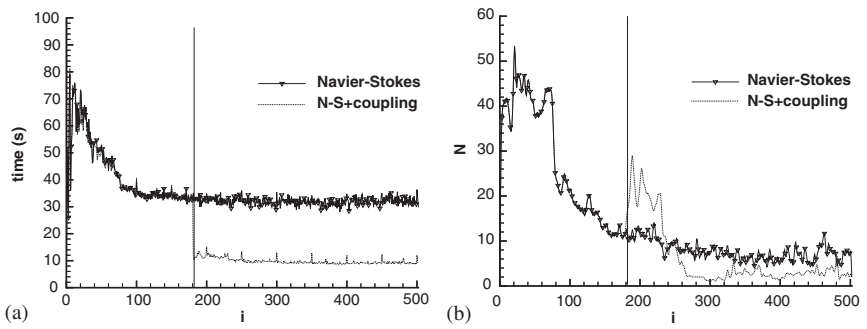

Figure 11. CPU time and solver iterations by time step: (a) CPU time, (b) solver iterations.

6. CONCLUSION

This paper deals with a new coupling approach for viscous–potential coupling. In the inner viscous domain, RANSE are solved with a fully coupled velocity, pressure and free-surface elevation method, while the Fourier–Kochin formulation of the Green function is used to compute potential flow in the outer domain. The great advantage of the Fourier–Kochin approach lies in the use of the three components of the viscous velocity-field to compute the external potential flow. So this method is very well suited to viscous–potential coupling. A strong coupling between the two domains is performed; at every time step the coupling algorithm is used to compute new boundary conditions for the viscous solver.

Computations were successfully performed on the steady ship-wave problem. This study shows stability of the coupling algorithm and that the coupling method computes far-field waves without disturbing the viscous flow closed to the hull. Moreover, influence of inner and outer surfaces locations is studied which allow us to select coupling surfaces following (i) the number of grid-point per wavelength in the viscous domain on the inner coupling surface and (ii) the wavelength for the outer coupling surface.

Main advantages of this approach are (i) CPU time decreasing, indeed CPU time per time iteration is divided by a factor 2 or 3 when the coupling approach is used, and (ii) a better computation of far-field waves, since the potential-flow theory avoids numerical damping dues to grid stretching away from the hull.

Further numerical computations are needed in order to valid this method. Computations on C–O or H–H grids will be investigated in order to get coupling surfaces which do not cut the wake. Thus, the wake will be compute by the Navier–Stokes solver which shall lead to more accurate computations and will allow us to use the present coupling method for numerous Froude number.

Nevertheless this study show abilities of strong viscous–potential coupling by the Fourier–Kochin method to solve wave resistance problems.

REFERENCES

1. Larsson L, Stern F, Bertram V. *A Workshop On Numerical Ship Hydrodynamics*. Gothenburg, Sweden, 2000.
2. Alessandrini B, Delhommeau G. A multigrid velocity–pressure–free surface elevation fully coupled solver for calculation of turbulent incompressible flow around a hull. *Proceedings of the 21st ONR Symposium on Naval Hydrodynamics*, Trondheim, 1996.

3. Chen X-B, Noblesse F. Green functions and super Green functions in free-surface hydrodynamics. *EUROMECH*, Poitiers, 1998.
4. Noblesse F, Yang C. Fourier–Kochin formulation of wave diffraction–radiation by ships or offshore structures. *Ship Technology Research* 1995; **42**:115–139.
5. Tahara Y, Stern F. Validation of an iterative approach for calculating ship boundary layers and wakes for nonzero Froude number. *Computers & Fluids* 1994; **23**:785–816.
6. Campana E, Di Mascio A, Esposito PG, Lalli F. Viscous-inviscid coupling in free surface ship flows. *International Journal for Numerical Methods in Fluids* 1995; **21**:699–722.
7. Chen H-C, Lin W-M, Weems K-M. Interactive zonal approach for ship flows including viscous and nonlinear wave effects. *Computers & Fluids* 1994; **23**.
8. Kang C-H, Chen H-C. Chimera RANS/laplace simulation of free surface flows induced by 2D ship sway, heave and roll motions. *Proceedings of the 8th ISOPE Conference*, Montreal, Canada, 1998.
9. Chen H-C, Lee S-K. RANS/laplace calculations of nonlinear waves induced by surface-piercing bodies. *Journal of Engineering Mechanics* 1999; **125**:1231–1242.
10. Menter FR. Zonal two equation k–ω turbulence models for aerodynamics flows. *Proceedings of the Fluid Dynamics Conference*, Vol. 1, Orlando, 1993.
11. Wilcox DC. Reassessment of the scale determining equation for advanced turbulence models. *AIAA Journal* 1988; **26**:1299–1310.
12. Wilcox DC. Multiscale model for turbulence flows. *AIAA Journal* 1988; **26**:1311–1320.
13. Alessandrini B, Delhommeau G. A multigrid velocity–pressure–free surface elevation fully coupled solver for turbulent incompressible flow around a hull. *Proceedings of the 9th International Conference on Numerical Methods in Laminar and Turbulent Flow*, vol. 1, Atlanta, 1995.
14. Rhie CM, Chow WL. Numerical study of the turbulent flow past an airfoil with trailing edge separation. *AIAA Journal* 1983; **21**(11):1525–1532.
15. Chen X-B, Noblesse F. Super Green functions. *Proceedings of the 22nd Symposium on Naval Hydrodynamics*, Washington, USA, 1998.
16. Noblesse F, Chen X-B. Decomposition of free-surface effects into wave and near-field components. *Ship Technology Research* 1995; **42**:167–185.
17. Kochin NE. On the wavemaking resistance and lift of bodies submerged in water. *Technical Report*, 1937 (translated in SNAME Tech. and Res. Bull. 1951:1–8).
18. Kochin NE. The theory of waves generated by oscillations of a body under the free surface of a heavy incompressible fluid. *Technical Report*, 1940 (translated in SNAME Tech. and Res. Bull. 1952:1–10).
19. Guillerm P-E. Application de la méthode de Fourier–Kochin au problème du couplage fluide visqueux-fluide parfait. *Thèse de doctorat*, Ecole Centrale de Nantes, 2001.
20. Yang C, Löhner R, Noblesse F. Farfield extension of nearfield steady ship waves. *Ship Technology Research* 2000; **47**:22–34.
21. Stern F, Toda Y, Longo J. *IIHR Report 352*. Iowa Institute of Hydraulic Research, University of Iowa, USA, 1991.
22. Mori K, Hinatsu M. Review of program 1 viscous flow around series 60 with free-surface. *CFD Workshop Tokyo*, vol. 2, Ship Research Institute, 1994.

